

Comparison of individual versus ensemble wind farm parameterizations inclusive of sub-grid wakes for the WRF model

*Original*

Comparison of individual versus ensemble wind farm parameterizations inclusive of sub-grid wakes for the WRF model / Ma, Yulong; Lozej Archer, Cristina; Vassel-Be-Hagh, A.. - In: WIND ENERGY. - ISSN 1095-4244. - 25:9(2022), pp. 1573-1595. [10.1002/we.2758]

*Availability:*

This version is available at: 11583/3008455 since: 2026-03-09T20:53:35Z

*Publisher:*

Wiley

*Published*

DOI:10.1002/we.2758

*Terms of use:*

This article is made available under terms and conditions as specified in the corresponding bibliographic description in the repository

*Publisher copyright*

(Article begins on next page)

## RESEARCH ARTICLE

WILEY

# Comparison of individual versus ensemble wind farm parameterizations inclusive of sub-grid wakes for the WRF model

Yulong Ma<sup>1</sup> | Cristina L. Archer<sup>1</sup>  | Ahmad Vasel-Be-Hagh<sup>2</sup>

<sup>1</sup>Center for Research in Wind (CRew),  
University of Delaware, Newark, Delaware,  
USA

<sup>2</sup>Fluid Mechanics Research Laboratory,  
Mechanical Engineering Department,  
Tennessee Tech University, Cookeville,  
Tennessee, USA

## Correspondence

Cristina L. Archer, Integrated Science and  
Engineering Laboratory (ISELab), University of  
Delaware, 221 Academy St, Newark, DE  
19716, USA.

Email: [carcher@udel.edu](mailto:carcher@udel.edu)

## Funding information

U.S. Bureau of Ocean Energy Management  
(BOEM), Grant/Award Number: 0040420490

## Abstract

Wind turbine wakes can be predicted somewhat accurately with mesoscale numerical models, such as the Weather Research and Forecast (WRF) model, via a wind farm parameterization (WFP) that treats the effects of the wakes, which are sub-grid features, on power production and the environment. A few WFPs have been proposed in the literature, but none has been able to properly account for the individual wakes within a grid cell or the effects of overlapping wakes from multiple turbines. A solution to these two issues is a WFP that includes both a wake model, which is a simplified analytical model of the wind speed (or wind power) deficit caused by a wake, and a wake superposition model, which accounts for overlapping wakes. Several such WFPs are developed here for the WRF model—based on the Jensen, the Geometric, and the Gaussian wake models coupled with two wake superposition methods (based on a squared deficit and a squared velocity superposition)—and tested individually, as well as combined together in an ensemble (EWFP), at two modern offshore wind farms. Most WFPs perform satisfactorily alone, but the EWFP generally outperforms them at both farms. The issue of resolved versus sub-grid wakes is explored for single- and multi-cell cases and for directions of alignment and non-alignment between the wind direction and the turbine columns. Although different combinations of wake loss and wake superposition models might be preferred at other wind farms, the general findings and detailed performance statistics given here might provide useful guidance in their selection.

## KEYWORDS

Anholt, Jensen, Lillgrund, wake effects, wake losses, wind turbine, WRF

## 1 | INTRODUCTION

In the last decade, the global wind power market has experienced tremendous growth, with a quadrupling of the installed wind capacity.<sup>1</sup> Despite the impacts of COVID-19, the year 2020 was a record year for wind power, with about 93 Gigawatts (GW) of new capacity installed,

**Abbreviations:** EWFP, ensemble wind farm parameterization; GM, geometric model; WFP, wind farm parameterization; WRF, Weather Research and Forecast model; XA, Xie and Archer (2015).

This is an open access article under the terms of the [Creative Commons Attribution-NonCommercial-NoDerivs](https://creativecommons.org/licenses/by-nc-nd/4.0/) License, which permits use and distribution in any medium, provided the original work is properly cited, the use is non-commercial and no modifications or adaptations are made.

© 2022 The Authors. *Wind Energy* published by John Wiley & Sons Ltd.

corresponding to a 53% increase with respect to the previous year.<sup>1</sup> This phenomenal growth has been achieved via increasingly larger wind farms, with dimensions that can be considered intermediate in atmospheric scales. For instance, the Horse Hollow Wind Energy Centre in Texas covers an area of 240 km<sup>2</sup>,<sup>2</sup> comparable to a typical thunderstorm cell. A second trend is that high wind speed areas have become inevitably crowded with multiple neighboring wind farms, often separated by only a few miles. For example, the Rødsand I and II offshore wind farms, located south of the island of Lolland in the Baltic Sea, are approximately 10 km apart. Hence, it is vital to have accurate computational tools for predicting the two-way turbine-to-turbine and farm-to-farm aerodynamic interactions in order to design efficient wind farms. Applying intermediate scale (mesoscale) models to forecast the wake characteristics and wind power production has become increasingly popular to address this need.<sup>3</sup> A mesoscale model that appears to be effective at carrying this task is the Weather Research and Forecasting (WRF) model, initially developed for atmospheric research and operational weather forecasting.<sup>4</sup>

To employ the WRF model for wind power forecasts, a simplified representation of the wind turbine effects and their interactions with the atmospheric flow needs to be incorporated in the model. This simplified representation is called a wind farm parameterization (WFP). A WFP is necessary because the grid resolution of typical mesoscale simulations is of the order of 10 km or larger, while the resolution required to resolve the flow features around the turbines would be of the order of a few meters. The most widely used WFP for the WRF model is the Fitch parameterization,<sup>5</sup> which models the wind turbines as momentum sinks that convert the mean kinetic energy of the air flow into electrical power and turbulent kinetic energy (TKE). Because the Fitch parameterization is incorporated in the WRF release since version 3.3, it has been the most widely used to investigate wake characteristics and power production of wind farms (e.g., Pryor et al.,<sup>6</sup> Prosper et al.,<sup>7</sup> Siedersleben et al.,<sup>8</sup> Boezio and Ortelli,<sup>9</sup> Duarte Jacondino et al.,<sup>10</sup> among others). However, as Pan and Archer<sup>11</sup> discussed, this parameterization suffers from a few shortcomings: it ignores the wakes of turbines that are in the same computational cell, leading to an over-estimation of the wind farm power production (also see Wang and Jin<sup>12</sup>); it is insensitive to the turbine positions in a grid cell (i.e., the power output is the same regardless of where the turbines are positioned); and it is insensitive to wind direction when the entire wind farm is contained in a single grid cell (i.e., the power output of the farm is the same for all wind directions, including directions of non-alignment). In addition, the treatment of TKE has been inaccurate up to WRF v. 4.1, with too much TKE in the grid cells with turbines and too little in the downstream grid cells.<sup>13</sup> As such, the Fitch parameterization is recommended at high resolution (order of 1 km or five turbine diameters) and when only a few turbines are present in each grid cell.<sup>13,14</sup> At coarser resolutions, which have been the most common in the literature, the Fitch parameterization generally largely over-estimates the power production of a wind farm,<sup>15,16</sup> that is, a positive bias.

A few additional WFPs have been proposed since Fitch's, but so far none has been officially incorporated in the WRF model. For example, Adams and Keith<sup>17</sup> proposed a WFP for the WRF model that is very similar to Fitch's and applied it to a large hypothetical wind farm over the US Midwest.<sup>18</sup>

Another WFP is the Explicit Wake Parameterization (EWP) by Volker et al.,<sup>19</sup> which adds a new term to the TKE equation to explicitly account for the TKE added by the wind turbines within a grid cell. The EWP assumes that every turbine within a grid cell is positioned at its center; hence, it does not consider their sub-grid interactions or the effect of the turbine layout. Only the vertical expansion of the sub-grid wakes is accounted for. At every time step, it obtains the total thrust force within a grid cell via a linear addition of each turbine's thrust force. By using the grid cell velocity at hub height as the upstream velocity for all turbines within the same grid cell, the EWP effectively ignores the velocity deficit that upstream turbines within a grid cell impose on their downstream counterparts. The EWP tends to predict weaker wind speed deficits and shorter wakes than Fitch's,<sup>20</sup> thus potentially introducing even higher positive biases in power production.

Mayol et al.<sup>21</sup> proposed a modified version of the Fitch parameterization, namely the Induction Aware Wind Farm Parameterization (IAWFP). IAWFP is made aware of the induction zone produced by the parameterized wind turbines by working with a "reference velocity" instead of the speed in the grid cell that contains the wind turbine. The authors compared the performance of IAWFP against the old and the corrected<sup>13</sup> implementations of the Fitch and the EWP. They found that IAWFP imposed the most significant deficits at hub height while the EWP was the one that reported the lowest values. Note that IAWFP also suffers from assuming that all the turbines are located at the grid cell's center, thus ignoring the turbine layout in a grid cell.

In addition to the parameterizations described above, researchers have proposed coupling the WRF model with the Fitch parameterization to large-eddy simulations (LES).<sup>22</sup> This method requires that the mesh be refined five times, downscaling from 4 km by 4 km to 4 m by 6 m grid cells. While this coupling technique addresses the main issue of employing the Fitch parameterization for investigating wind farm wakes, it is computationally costly.

Some recent studies have proposed combining WRF output data with field measurements, including lidars and meteorological masts. Elshafei et al.,<sup>23</sup> for instance, proposed using deep multi-fidelity Gaussian regression and non-linear autoregression to respectively perform temporal and spatial data fusion to combine intermittent field measurement data and continuous WRF results. While this method appears to increase the accuracy of WRF's output, it requires access to field-measured data, which are not widely available, especially for the case of future or planned wind farms, and are expensive to collect.

One can conclude that the use of mesoscale models, such as WRF, for wind farm applications is hindered by the lack of a parameterization that realistically accounts for the wakes of individual wind turbines but is not as computationally costly as LES or as inaccessible as field measurements. The solution that we propose here is to incorporate "analytical" wake loss models, also called "kinematic" models, into WFPs for the WRF

model. These models provide an analytical solution to the local wind speed deficit (or the local power production) caused by an upstream turbine.<sup>24</sup> Using such models enables WRF to take into account the exact location of each turbine within every grid cell and their aerodynamic interactions. A wake superposition technique then combines the wind speed deficit caused by each upstream turbine to obtain the overall deficit at every point within the domain.

Two analytical wake loss models have already been proposed for WRF in the literature: the hybrid parameterization by Pan and Archer<sup>11</sup> and the Jensen parameterization by Ma and Archer.<sup>16</sup> The hybrid WFP directly accounts for the effect of turbine layout and wind direction by calculating the wake losses at each grid cell using the geometric wake loss model by Ghaisas and Archer.<sup>25</sup> The hybrid parameterization was shown to be more accurate than the Fitch's at simulating the power production of the Lillgrund offshore wind farm, which comprises 48 Siemens 2.3 MW turbines; however, it has not been tested at wind farms that use a different turbine model. The Jensen WFP uses the well-known Jensen wake loss model,<sup>26</sup> which assumes a linear expansion of the wind turbine wake and a top-hat wind speed deficit profile to calculate wake losses. The Jensen WFP was shown to be more accurate than Fitch's at two wind farms, especially at coarse resolutions (larger than 4 km).<sup>16</sup> Both the geometric model (GM) and the Jensen wake loss model will therefore be included in this study. A third analytical wake loss model, the Gaussian model by Xie and Archer,<sup>27</sup> referred to as XA hereafter, was also shown to be effective at predicting the power output at three wind farms,<sup>24</sup> but it has never been incorporated in the WRF model prior to this study. Hence, the objective of this article is to evaluate the effectiveness of the mentioned three WFPs for WRF based on three wake loss models—the Jensen, GM, and XA models—as well as that of their “ensemble,” meaning the average of the three wake loss model results, referred to hereafter as EWFP. Four different wake superposition methods will also be compared (M1,<sup>28</sup> M2,<sup>26</sup> M3,<sup>29</sup> and M4<sup>16</sup>) to identify the most efficient way to combine the impact of upstream turbines. In the rest of this paper, the term WFP will indicate the combination of a wake loss model and a wake superposition method.

## 2 | METHODS

Of the three wake models used in this study, Jensen and XA provide an estimate of the wind speed deficit caused by a wind turbine, while the GM estimates the power production of each turbine directly. Here we review first the main equations used in the Jensen and XA models (Sections 2.1 and 2.2), including four wake superposition methods (Section 2.3), and then introduce the GM model (Section 2.4).

In general, the normalized wind speed deficit is:

$$\delta = \frac{\Delta U}{U_\infty} = \frac{U_\infty - U}{U_\infty}, \quad (1)$$

where  $U_\infty$  is the undisturbed hub-height wind speed,  $U$  is the (reduced) hub-height wind speed in the wake, and  $\Delta U$  is the wind speed deficit.

### 2.1 | The Jensen model

The Jensen wake model assumes that the wake is laterally finite (i.e., it has an outer edge), that the wake expands linearly as a function of the downwind distance  $x$  from the turbine only, and that the normalized wind speed deficit follows a top-hat distribution as follows:

$$\delta = \delta(x) = \left[ \frac{2a}{(1 + 2k_w \frac{x}{D})^2} \right], \quad (2)$$

where  $D$  is the turbine diameter,  $k_w$  is the dimensionless rate of wake expansion, equal to 0.075<sup>26</sup> and 0.04<sup>30</sup> for onshore and offshore wind farms, respectively, and the induction factor  $a$  is related to the thrust coefficient  $C_T$  by:

$$a = \frac{1 - \sqrt{1 - C_T}}{2}. \quad (3)$$

We note that  $C_T$  is a function of  $U_{in}$ , which is the (incoming) hub-height wind speed experienced by the turbine. If the turbine is in the front row, then  $U_{in} = U_\infty$ , otherwise  $U_{in}$  is lower due to the turbine's exposure to the upstream wakes.

The hub-height wind speed at turbine  $i$  caused by the wake of turbine  $j$  is expressed as:

$$U_{ij} = U_\infty (1 - \delta_{ij}) = U_\infty \left[ 1 - \frac{2a}{(1 + 2k_w \frac{x_j}{D})^2} \right], \quad (4)$$

where  $x_{ij}$  is the along-wind distance between turbines  $i$  and  $j$ .

If turbine  $i$  with rotor area  $A_i$  is not perfectly aligned with the upstream turbine  $j$  along the wind direction, the Jensen model needs a modification to account for the fact that only a portion of its rotor ( $A_{0,ij}$ ) is affected by the wake of turbine  $j$ , while the rest of the rotor ( $A_i - A_{0,ij}$ ) experiences the undisturbed wind speed  $U_\infty$ <sup>24</sup>:

$$U_{ij} = U_\infty \frac{A_i - A_{0,ij}}{A_i} + U_\infty (1 - \delta_{ij}) \frac{A_{0,ij}}{A_i} = U_\infty - \delta_{ij} U_\infty \frac{A_{0,ij}}{A_i}. \quad (5)$$

The wind speed provided by Equation (5) is effectively a rotor-average wind speed (also known as rotor-equivalent or rotor-layer wind speed), which is a better representation of the wind speed experienced by the entire rotor than the wind speed at the exact location of the hub, and ultimately provides a better estimate of the power production of the turbine.<sup>31,32</sup>

Note that Equation (5) assumes that the undisturbed wind speed  $U_\infty$  is the same for turbines  $i$  and  $j$ . This is true in single-cell cases, where all the turbines are in the same grid cell. However, in multi-cell cases, turbines  $i$  and  $j$  may be located in different grid cells and therefore may experience different undisturbed wind speeds. A more general expression for Equation (5), valid in multi-cell cases, is:

$$U_{ij} = U_{\infty,i} \frac{A_i - A_{0,ij}}{A_i} + U_{\infty,j} (1 - \delta_{ij}) \frac{A_{0,ij}}{A_i}. \quad (6)$$

## 2.2 | The XA model

The XA wake model, developed by Xie and Archer,<sup>27</sup> predicts a wake that is neither axis-symmetric nor conical, but ellipsoidal. The wind speed deficit in the XA model is a Gaussian function of  $x$ ,  $y$ , and  $z$ , defined as:

$$\delta = \delta(x, y, z) = \delta_{hub} \exp \left\{ - \left[ \frac{(z-H)^2}{2\sigma_z^2} + \frac{y^2}{2\sigma_y^2} \right] \right\}, \quad (7)$$

$$\delta_{hub} = \delta_{hub}(x) = 1 - \sqrt{1 - \frac{C_T}{8 \frac{\sigma_y \sigma_z}{D^2}}}, \quad (8)$$

$$\frac{\sigma_y}{D} = \frac{\sigma_y(x)}{D} = k_y \frac{x}{D} + \varepsilon, \quad (9)$$

$$\frac{\sigma_z}{D} = \frac{\sigma_z(x)}{D} = k_z \frac{x}{D} + \varepsilon, \quad (10)$$

where  $k_y = 0.025$  and  $k_z = 0.0175$  are the dimensionless growth rates of the wake in the  $y$  and  $z$  directions, obtained from a fit to LES results of a single turbine wake under neutral stability,<sup>27</sup>  $\varepsilon = 0.25\sqrt{\beta}$ ,  $\beta = 0.5(1 + \sqrt{1 - C_T}/\sqrt{1 - C_T})$ , and  $C_T = C_T(U_{in})$ .

Whereas the wake predicted with the Jensen model is finite, meaning that it has a clear edge, Gaussian wakes are infinite, at least in principle; thus, any wake will always impact the entire rotor of any downstream turbine. As such, the wind speed at turbine  $i$  caused by turbine  $j$  with the XA model in the multi-cell cases is:

$$U_{ij} = U_{\infty,j} - \frac{\int_{A_i} \delta_{ij} U_{\infty,j} dA}{A_i}, \quad (11)$$

where  $\delta_{ij}$  is given by Equation (7) after replacing  $x$  with  $x_{ij}$ . The single-cell equivalent can be obtained by replacing  $U_{\infty,j} = U_{\infty,i} = U_\infty$ . Because of the Gaussian curve properties, the integral in Equation (11) can be solved analytically.<sup>33</sup>

## 2.3 | Wake superposition methods

When multiple wakes from multiple turbines  $j$  ( $j = 1 \dots N$ ) overlap at turbine  $i$ , the incoming wind speed for turbine  $i$  needs to be calculated by a wake superposition method. A review of different methods is given in Porté-Agel et al.<sup>34</sup> The two most common superposition methods of wind speed deficits are a linear superposition,<sup>28</sup> called method M1 hereafter:

$$M1: U_i = U_{\infty,i} - \sum_{j=1}^N \left[ \delta_{ij} U_{\infty,j} \frac{A_{0,ij}}{A_i} \right], \quad (12)$$

and a squared superposition,<sup>26</sup> called method M2 hereafter:

$$M2: U_i = U_{\infty,i} - \sqrt{\sum_{j=1}^N \left[ \delta_{ij} U_{\infty,j} \frac{A_{0,ij}}{A_i} \right]^2}. \quad (13)$$

The formulations of the superposition methods M1 and M2 for the XA model are:

$$M1: U_i = U_{\infty,i} - \sum_{j=1}^N \left[ \frac{\int_{A_i} \delta_{ij} U_{\infty,j} dA}{A_i} \right] \quad (14)$$

and

$$M2: U_i = U_{\infty,i} - \sqrt{\sum_{j=1}^N \left[ \frac{\int_{A_i} \delta_{ij} U_{\infty,j} dA}{A_i} \right]^2}. \quad (15)$$

At the upwind turbine  $j$ , the incoming wind speed  $U_j$  is not necessarily equal to the undisturbed wind speed  $U_{\infty,j}$ , since turbine  $j$  itself may also be affected by wakes. As such, an alternative method,<sup>29</sup> named M3 hereafter, can be used in the Jensen model to estimate  $U_i$  based on a slight modification of Equation (13) as follows:

$$M3: U_i = U_{\infty,i} - \sqrt{\sum_{j=1}^N \left[ \delta_{ij} U_j \frac{A_{0,ij}}{A_i} \right]^2}. \quad (16)$$

For the XA model, the equation for method M3 becomes:

$$M3: U_i = U_{\infty,i} - \sqrt{\sum_{j=1}^N \left[ \frac{\int_{A_i} \delta_{ij} U_j dA}{A_i} \right]^2}. \quad (17)$$

Lastly, Ma and Archer<sup>16</sup> proposed a new wake overlap method, named M4, that is based on the superposition of not the wind speed deficits, but the resulting wind speeds ( $U_{ij}$ ) at turbine  $i$  from each wake  $j$  as follows:

$$M4: U_i = \sqrt{\frac{\sum_{j=1}^N U_{ij}^2}{N}}, \quad (18)$$

where  $U_{ij}$  is given by Equation (6) and Equation (11) in the Jensen and the XA models, respectively. Note that, in single-cell cases,  $U_{\infty,j} = U_{\infty,i} = U_{\infty}$  in Equations (12)–(18). Method M4 was developed specifically to better take into account large- and mesoscale wind speed variability inside a wind farm, like that caused by a weather storm approaching a wind farm. As such, M4 is expected to perform better in multi- than single-cell

cases, as single-cell cases do not have any wind speed variability within the wind farm by definition (except for that caused by the wakes themselves).

The power generated by turbine  $i$  can then be calculated, for both Jensen and XA models, by inserting the value of  $U_i$  in the power curve provided by the manufacturer. Wind direction variability within the wind farm in the multi-cell case is treated as in Ma and Archer.<sup>16</sup>

Methods M1 and M2 performed poorly when compared against methods M3 and M4 in the Jensen model. The average RMSE of M1 and M2 was 22.5% and 16.1% at Lillgrund for single-cell cases, compared with 9.0% and 10.1% for M3 and M4. As such, M1 and M2 will not be further considered in this study.

## 2.4 | The geometric model (GM)

The GM estimates the relative power generated by any downstream turbine with respect to the power generated by the upstream turbine.<sup>25</sup> The GM is a hybrid wake model because it does not simulate the physical processes occurring in wakes, like the wake expansion, but rather uses empirical coefficients, derived from a multi-linear regression, to relate the power production of a wind turbine in a wind farm to two geometric quantities: blockage ratio and blockage distance.<sup>11,25</sup>

The blockage ratio  $BR_i$  of a wind turbine  $i$  for a given wind direction is the fraction of the swept area of turbine  $i$  that is blocked by the swept area of any upstream turbine ( $0 < BR_i < 1$ ). A blockage ratio of 0 for a given wind direction means that the turbine is not blocked at all and receives the undisturbed wind speed  $U_\infty$  in that direction. A blockage ratio of 1 means that the turbine is completely blocked by one or more upstream wind turbines. Hence, the relative power production of a wind turbine decreases with its blockage ratio. Most turbines are partially blocked.

The blockage distance  $BD_i$  is a measure of the distance between the wind turbine  $i$  and the upstream blocking turbines. Hence, a larger blockage distance means a greater wind speed recovery, lower wake losses, and consequently more power production; vice versa, a small blockage distance is associated with high wake losses and low power production.

The  $BR_i$  and  $BD_i$  for a given wind direction are defined as:

$$BR_i = \frac{1}{A_i} \int_{A_i} \chi dA; \quad (19)$$

$$BD_i = \frac{1}{A_i} \int_{A_i} [\chi L + (1 - \chi)L_\infty] dA; \quad (20)$$

where  $\chi = 1$  if the infinitesimal element of swept area  $dA$  of turbine  $i$  that is blocked by a turbine and  $\chi = 0$  otherwise, and  $L$  denotes the distance of the element  $dA$  to the upstream blocking turbine. Wherever  $\chi = 0$ , that portion of the swept area of turbine  $i$  is not blocked by any other turbine and  $L$  is assigned an arbitrary large value  $L_\infty$  ( $L_\infty = 20D$  was used here). The blockage distance may be thought of as the weighted average of the distances between turbine  $i$  and all turbines  $j$  that are upstream of turbine  $i$ , weighted by the fraction of area blocked by each.

In the original formulation of the GM, the wind speed deficit is skipped entirely and the relative power  $P_{R,i}$  is provided directly as a function of  $BR_i$  and  $BD_i$  as follows:

$$P_{R,i} = \frac{P_i}{P_0} = \begin{cases} \alpha + \beta BR_i + \gamma \frac{BD_i}{L_\infty} & BR_i \neq 0, \\ 0 & BR_i = 0, \end{cases} \quad (21)$$

where  $P_i$  and  $P_0$  are the power generated by turbine  $i$  and by the front turbine, and the fitting coefficients  $\alpha$ ,  $\beta$ , and  $\gamma$  are equal to 0.6824, -0.3405, and 0.2131, respectively. These coefficients were derived by multiple linear regression between the turbine power simulated in a suite of LES based on the Lillgrund wind farm and the values of  $BR_i$  and  $BD_i$  for several wind directions.<sup>25</sup> Despite being simple geometric properties, with no assumption on the shape or strength of the wake,  $BR_i$  and  $BD_i$  correlated extremely well with the simulated relative power, with correlation coefficients in excess of 96% at Lillgrund.<sup>25</sup>

In this paper, however, we used the ratio of the local wind speed at the turbine over the undisturbed wind speed that was provided in the hybrid parameterization by Pan and Archer<sup>11</sup> as follows:

$$\frac{U_i}{U_{\infty,j}} = \begin{cases} \alpha + \beta BR_i + \gamma \frac{BD_i}{L_\infty} & BR_i \neq 0, \\ 1 & BR_i = 0, \end{cases} \quad (22)$$

where  $\alpha$ ,  $\beta$ , and  $\gamma$  are equal to 0.9615, -0.1549, and 0.0114, respectively. These coefficients were derived by Pan and Archer<sup>11</sup> using the same method and the same LES dataset used for the GM,<sup>25</sup> that is, by multiple linear regression between the LES wind speed at each turbine  $i$  and the values of  $BR_i$  and  $BD_i$ . The actual power  $P_i$  can then be calculated with the power curve of the wind turbine, typically provided by the manufacturer.

### 3 | DATA

The two wind farms analyzed in this study are Lillgrund and Anholt (Figure 1), which have been described in detail by Archer et al,<sup>24</sup> including the data cleaning procedures. Selecting these two farms allows for examining the performance of the proposed models at both structured and unstructured, as well as closely and widely spaced layouts.

#### 3.1 | Lillgrund

The Lillgrund offshore wind farm, located in the shallow waters (4–8 m) between Denmark and Sweden, was completed between 2006 and 2007 and is currently owned and operated by Vattenfall. It comprises 48 Siemens 2.3-MW wind turbines with rotor diameter  $D = 93$  m and hub height  $H = 65$  m, for an installed capacity of 110 MW. The layout of Lillgrund is regular (Figure 1A), meaning that the rows and columns are arranged along straight lines and the turbines are equally spaced along them, except for a “hole” near the middle of the farm, where unfavorable sea floor conditions prevented the installation of two turbines.

There are 10 directions of alignment at Lillgrund:  $0^\circ$ ,  $42^\circ$ ,  $75^\circ$ ,  $90^\circ$ ,  $120^\circ$ ,  $180^\circ$ ,  $222^\circ$ ,  $255^\circ$ ,  $270^\circ$ , and  $300^\circ$ . The two directions that define the regular grid of turbines are  $222^\circ$  and  $120^\circ$ , with axial spacing of  $4.3D$  and lateral spacing of  $3.3D$ . This spacing of  $4.3D \times 3.3D$  is the tightest of any utility-scale wind farm worldwide and therefore the wake losses are large. Thus, it was not possible to identify a true direction of non-

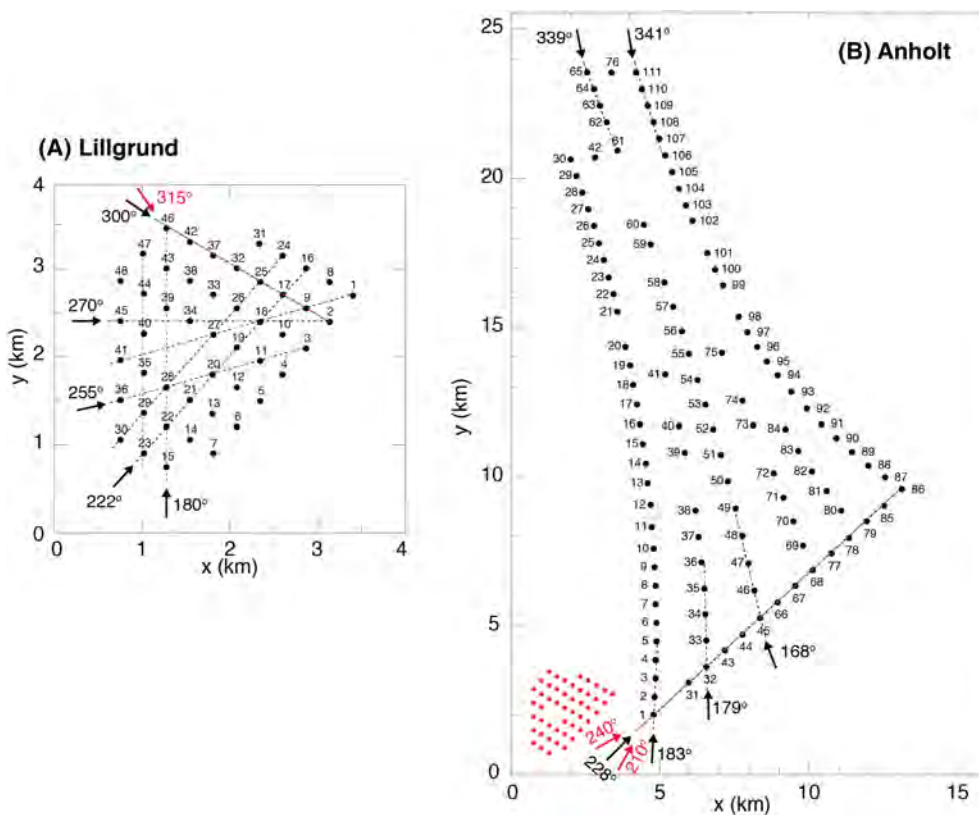


**FIGURE 1** Wind turbine layout at Lillgrund (A) and Anholt (B). The black dashed lines indicate the wind directions (black arrows) aligned with wind turbine columns. The red arrows indicate the directions of non-alignment. The red dashed lines are the columns analyzed in this study for the non-alignment directions<sup>16</sup>

alignment (i.e., with zero wake losses), but  $315^\circ$  was characterized by relatively small wake losses and therefore it was used here as a direction of non-alignment. The wind rose at hub height is shown in Figure 2A.

The dataset used in this study includes wind power, yaw angle, wind speed, rotational speed, and blade pitch angles of each turbine for approximately 16 months at a frequency of 1 minute or less.<sup>24</sup>

### 3.2 | Anholt

The Anholt offshore wind farm is located between Djursland and the island of Anholt in Denmark, in water depths of 15–19 m. It was built by Ørsted (formerly DONG Energy) between 2012 and 2013 with a unique irregular layout (Figure 1B). It hosts 111 Siemens 3.6-MW wind turbines with rotor diameter  $D = 120$  m and hub height  $H = 82$  m, for a total installed capacity of approximately 400 MW.

The dataset used in this study includes wind power, yaw angle, wind speed, rotational speed, and blade pitch angles of each turbine at a frequency of 10 minutes from January 2013 to June 2015.<sup>24</sup> Because the layout is irregular, it is impossible to define directions of alignment and non-alignment for all the turbines at Anholt. As such, only a few directions with as many turbines as possible aligned along them were identified:  $168^\circ$  (turbines 45–49),  $179^\circ$  (turbines 32–36),  $183^\circ$  (1–5),  $228^\circ$  (first row: 31, 31–32, 43–45, 66–68, 77–79, 85–86; and second row: 10, 38, 50, 84, 92), and  $341^\circ$  (21–30). The directions of non-alignment are  $210^\circ$  and  $240^\circ$ . The wind rose at hub height is shown in Figure 2B.

## 4 | NUMERICAL SIMULATIONS

In this study, all the simulations are performed with the WRF model under ideal atmospheric conditions, where the inflow wind speed and direction are kept constant. The idealized runs allow us to more clearly isolate the effects introduced by the changes in the wind farm parameterization. In addition, although we recognize that atmospheric stability may impact the evolution, shape, length, and duration of the wake, neither the Lillgrund nor the Anholt dataset included any measurements of atmospheric stability. As such, we did not include any stability information in this study and performed all the simulations under neutral conditions.

The computational domain is  $144 \text{ km} \times 144 \text{ km} \times 10 \text{ km}$  ( $x \times y \times z$ ) for all simulations except for the single-cell case at Anholt, which is  $600 \text{ km} \times 600 \text{ km} \times 10 \text{ km}$ . The vertical resolution is 4.4 m near the surface and stretched above, with a total of 62 levels, of which 4 levels below the rotor and 7 levels across the rotor. The horizontal resolution is  $\Delta x = 2 \text{ km}$  at both wind farms for the multi-cell cases and 4 km and 24 km for Lillgrund and Anholt, respectively, for the single-cell cases.

The bottom boundary is set as water body, which provides only the momentum flux calculated in the surface layer scheme (i.e., no sensible and latent heat fluxes from the surface). The lateral boundary conditions are open radiative conditions. The Coriolis parameter is set to  $1.11 \times 10^{-4} \text{ s}^{-1}$ , corresponding to a latitude of  $50^\circ\text{N}$ , with imposed geostrophic wind of  $u_g = 7.6 \text{ m s}^{-1}$  and  $v_g = 5.88 \text{ m s}^{-1}$ , corresponding to a steady state wind direction of  $225^\circ$  at 70 m (i.e., about the hub height). The initial temperature is constant 300 K below 900 m and linearly increases with height at a rate of  $3 \text{ K km}^{-1}$  above 900 m. The initial horizontal wind components are set equal to the geostrophic wind and the humidity is set to zero at all levels.

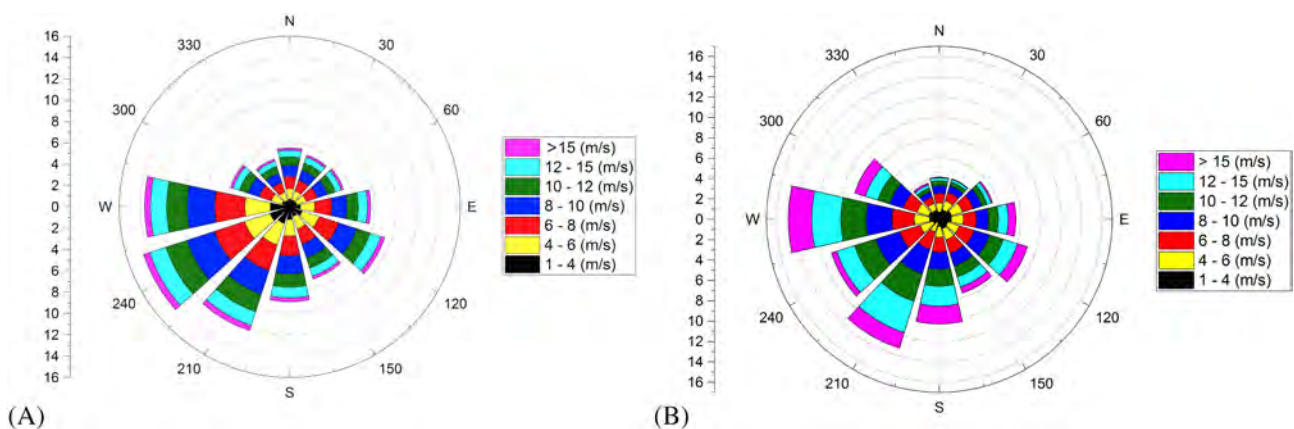


**FIGURE 2** Observed wind rose at hub height at (A) Lillgrund and (B) Anholt. The tick marks on the vertical axis correspond to the circles in the wind rose and represent the frequency of occurrence in percent. This figure was reproduced with permission from Figure 3 in Archer et al.<sup>24</sup>

Similar to the Fitch's, our proposed WFPs work only with the MYNN PBL scheme<sup>35</sup> in WRF; thus, the PBL scheme option `bl_pbl_physics` is set to 5. The simulations are integrated first for 96 hours without the turbines to reach a steady state. Then the wind farm is placed at the center of the domain and the simulations are run for another four hours. To account for the effects of different wind directions on the wind farm, the wind farm layout is rotated to the desired directions.

Horizontal directional shear across a multi-cell wind farm is taken into account via the method described in Ma and Archer<sup>16</sup>. In brief, each wake from each turbine in each upstream grid cell that affects a given wind turbine in a given grid cell is assumed to be aligned along a wind direction that is the average between that at the upstream grid cell and that at the given grid cell.

## 5 | RESULTS AND DISCUSSION

Each wake model—Jensen, XA, and GM—was applied at the two wind farms, for at least five directions of alignment and one of non-alignment, for single- and multi-cell cases, and with four wake superposition methods (except for the GM, which does not require wake superposition). As such, the goal of identifying which combination of wake model and wake superposition method performs best for which case required over 252 WRF simulations.

Examples of hub-height wind speed deficits simulated by the WRF model with a few selected WFPs (i.e., a combination of wake loss model and wake overlap method) and for the EWFP are given in Figures 3 and 4 for Lillgrund and Anholt, respectively, for both single- and multi-cell cases. The main patterns are rather similar among the WFPs, with the strongest deficits (up to 2.0 m/s) located within the farm or immediately downstream. The wakes of the farms—defined here as plume-like regions downwind of the wind farm with lower wind speed than the surrounding areas, without consideration for TKE—extend relatively far, order of 2–6 times the wind farm length along the wind direction. Without observations, it is impossible to determine which WFP produces the most realistic distribution of hub-height wind speed.

### 5.1 | Resolved versus sub-grid wakes

When it comes to numerical simulations of wind turbine wakes, there is an important distinction between “resolved” and “sub-grid” wakes. To understand the difference, consider a grid cell with wind turbines in it (Wind farm 1 in Figure 5). Any WFP predicts the power generated by all

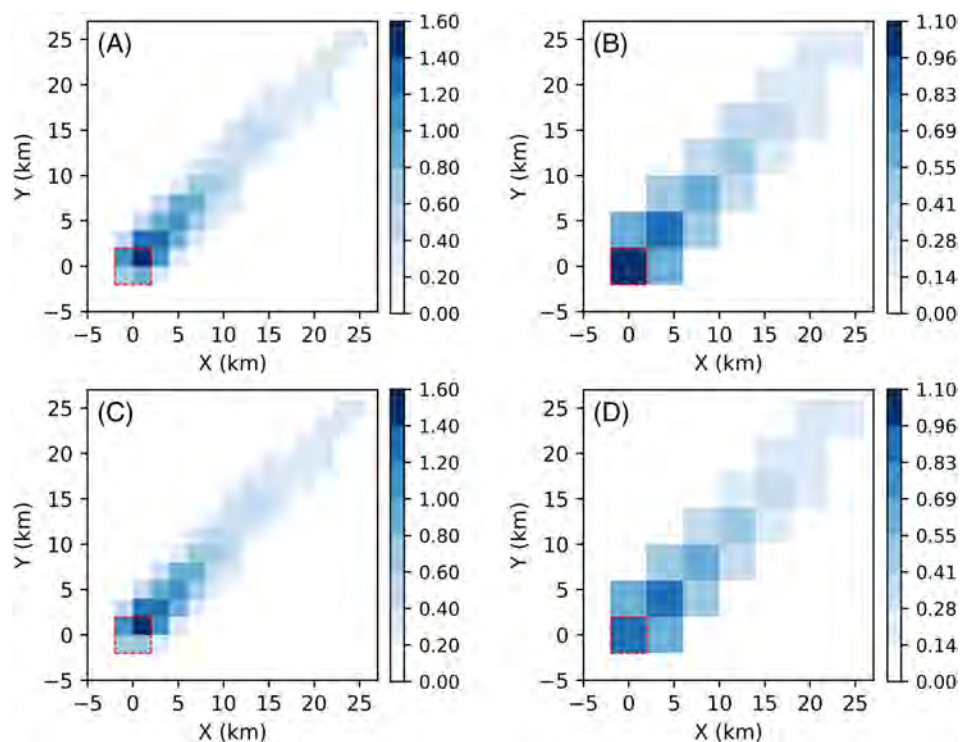


**FIGURE 3** Simulated hub-height (65 m) wind speed deficit (m/s) at Lillgrund for the 225° wind direction for the multi-cell cases at 2-km resolution (left) and the single-cell case at 4-km resolution (right) with: (A, B) GM and (C, D) the ensemble of JS-M4, XA-M3, and GM (EWFP). The wind farm is located in the lower left corner (red square).

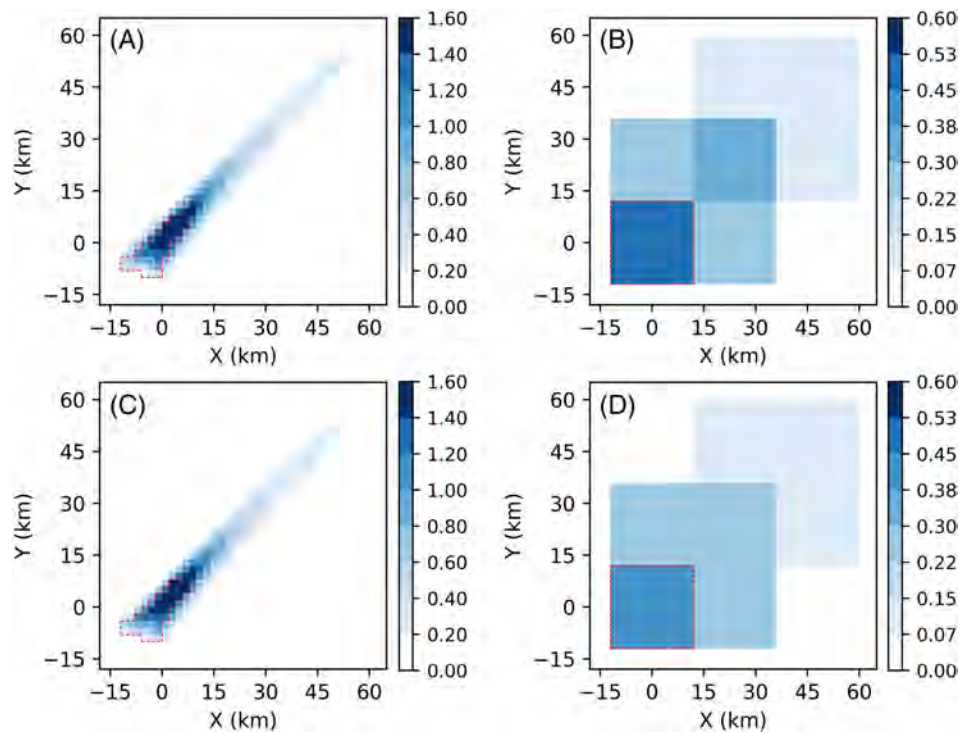


**FIGURE 4** Simulated hub-height (82 m) wind speed deficit (m/s) at Anholt for the 168° wind direction for the multi-cell cases at 2-km resolution (left) and the single-cell case at 24-km resolution (right) with: (A, B) JS-M4 and (C, D) the ensemble of JS-M4, XA-M3, and GM (EWFP). Note that the flow appears to be from the southeast, but in reality it is from 168° and the wind farm is rotated accordingly

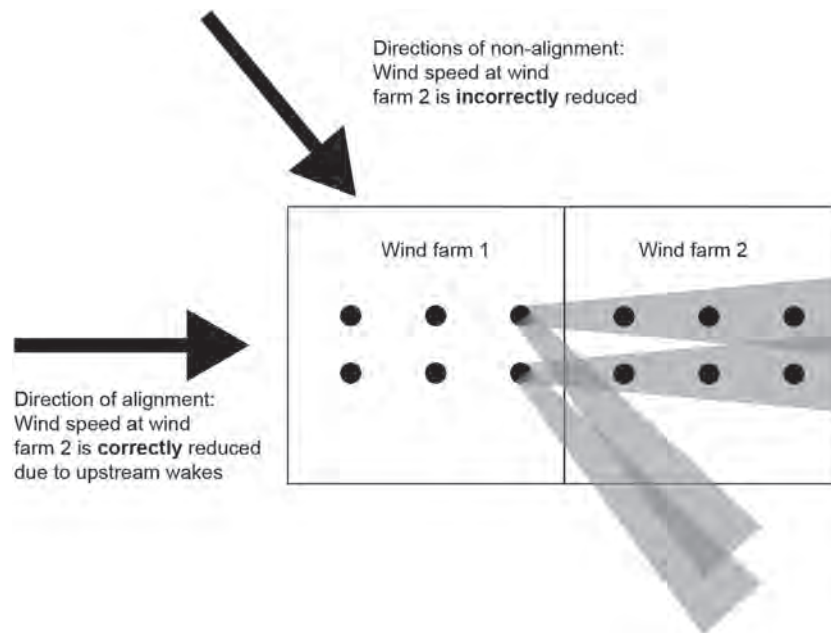


**FIGURE 5** The sub-grid wakes from Wind farm 1—only those from the last row of turbines are shown—may or may not impact the wind speed experienced by the turbines in Wind farm 2 depending on the alignment or non-alignment of the wind direction (black arrows) with the turbines, respectively.

the turbines in it, either via a treatment of the sub-grid wakes, as proposed here, or without considering the individual sub-grid wakes, as done in the Fitch's WFP. The WFP then updates the grid cell wind speed to a new value that is lower than that at the beginning of the time step. This lower wind speed is then advected to the grid cells downstream, where it is also affected by diffusion, turbulence, and entrainment, in a manner that can be thought of as a resolved wind farm wake<sup>16,36,37</sup> because no sub-grid processes are affecting it, only resolved-scale ones.

The single-cell cases provide examples for both sub-grid and resolved wakes (right column of Figures 3 and 4). The sub-grid wakes of the individual turbines within the farm are treated by the WFPs, including their superposition, and result in a lower value of wind speed at the grid cell of the wind farm than directly upstream. The wind speed deficit downstream of the wind farm is the resolved wake. There is no interference of one type of wake with the other in the single-cell cases and no double-counting of any wake effects because the sub-grid wakes are only treated in the grid cell of the wind farm, while the downstream wake is entirely resolved. By contrast, in the multi-cell cases (left column of Figures 3 and 4), since the proposed WFPs account for the sub-grid wakes in all grid cells, both types of wakes might be present simultaneously in the downstream grid cells.

Now imagine that another wind farm is placed in the grid cell immediately downwind of the original wind farm (Wind farm 2 in Figure 5). All the turbines in the new wind farm, even those that are in the front row, will experience a wind speed that is lower than the undisturbed wind speed upstream because the entire grid cell is affected by the resolved wake of the first wind farm. This wind speed is correctly lower if the turbines in the new wind farm are truly affected by the wakes of those upstream, that is, when they are aligned behind them (case of westerly flow in Figure 5), although not low enough because it is a grid-average wind speed, thus the wind speed deficit from the upstream wakes is diffused over the entire grid cell volume. But, if the turbines in the new wind farm are not affected by the upstream wakes, that is, in non-alignment cases (case of northwesterly flow in Figure 5), it is incorrectly lower because some/most of the turbines in the new wind farm are not affected by

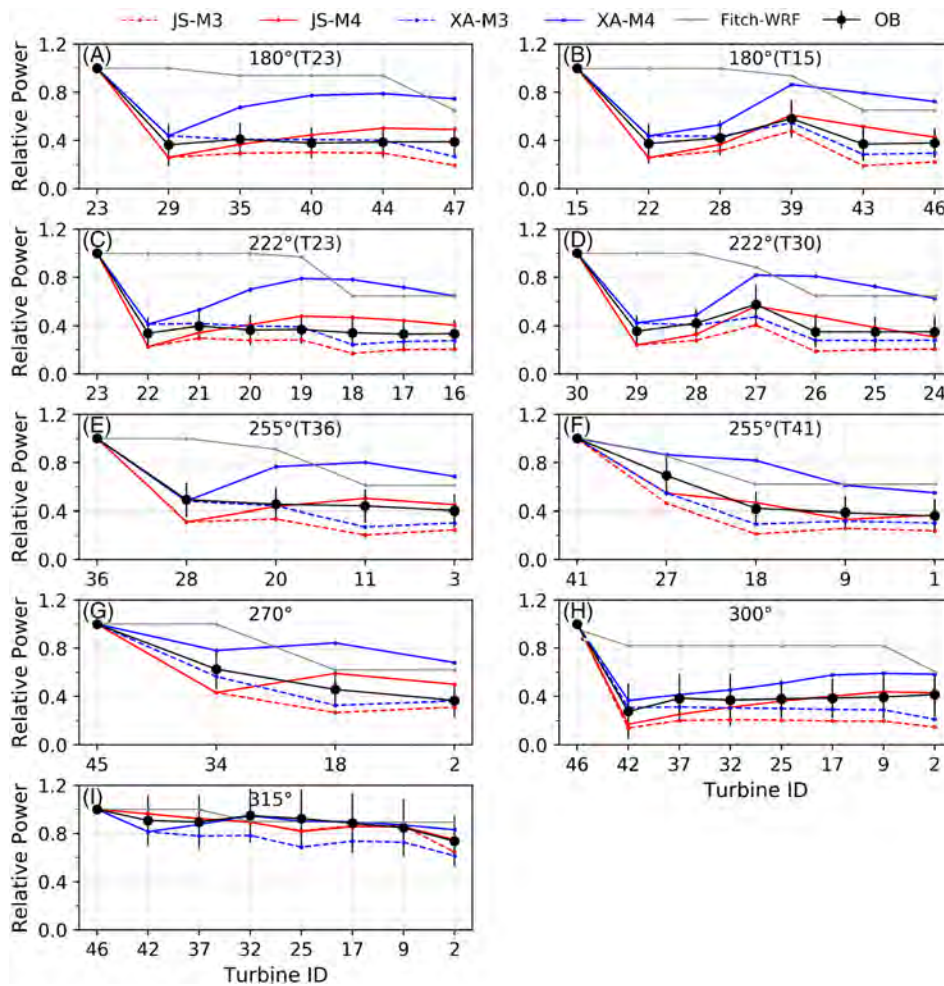


**FIGURE 6** Relative power at Lillgrund (multi-cell cases at 2-km resolution) from observations, from the Fitch parameterization, and from the Jensen and XA wake models with the two wake superposition methods M3 and M4 along the directions of alignment (A–H) and the direction of non-alignment 315° (I). The black circles represent the mean observed relative power and the bars are one standard deviation. The simulation results and the observations are averaged over a wind direction window of  $\pm 2.5^\circ$ .

upstream wakes and therefore should experience the same (high) undisturbed wind speed as the original wind farm. But, regardless of alignment or non-alignment and regardless of the treatment or non-treatment of the sub-grid wakes, due to the power extraction by the turbines, at the end of the time step the grid-average wind speed will be further reduced by the WFP in the downstream grid cell.

Now add even more turbines in further downstream cells. Even in the absence of a treatment of the sub-grid wakes (e.g., in the Fitch parameterization), the resolved wind speed will be reduced further in each additional downstream grid cell with turbines due to the power extraction, regardless of the relative position of the turbines. The continuous reduction of wind speed is never observed in reality, as relative power tends to plateau to a constant value after the first few rows of turbines, even for directions of perfect alignment.<sup>24,38,39</sup> The continuous reduction of wind speed (and relative power) in consecutive grid cells downstream is an unrealistic result of the resolved wake in multi-cell cases and can be observed in the results obtained with the Fitch parameterization in Figures 6 and 7 (gray lines).

Lastly, when the wind farm is partitioned over multiple grid cells, as in the multi-cell cases, and a WFP with sub-grid wakes is used, as done here, there is the possibility of both types of wakes being present simultaneously in the same grid cell, thus potentially double-counting some of the wake effects. When the Fitch WFP is used, the resolved wake is the only wake effect that is accounted for, but it is generally too weak. This explains why the Fitch WFP generally over-estimates power and underestimates the wind speed deficit, thus exhibits a strong positive bias (Figures 6 and 7). When the Jensen, XA, or GM parameterizations are used, however, the resolved wake is still present, but it is in addition to the sub-grid wakes, which are generally stronger. While for directions of alignment the resolved wake becomes more accurate with finer grid resolution (i.e., multi-cell cases) and with fewer turbines in each grid cell, for directions of non-alignment the power predictions are more accurate for single-cell cases (i.e., coarse resolution) because of the absence of the resolved wake effect. These issues related to resolved versus sub-grid wakes will become clearer after comparing single- and multi-cell results in the next sections.

## 5.2 | Wake superposition methods

We first focus on the wake superposition method, which was found to be as important as, if not more important than the wake model by Ma and Archer.<sup>16</sup> Since the GM does not provide an estimate of the wind speed deficit, only the Jensen and XA models will be compared in this section for the single- and multi-cell cases at Lillgrund and Anholt.

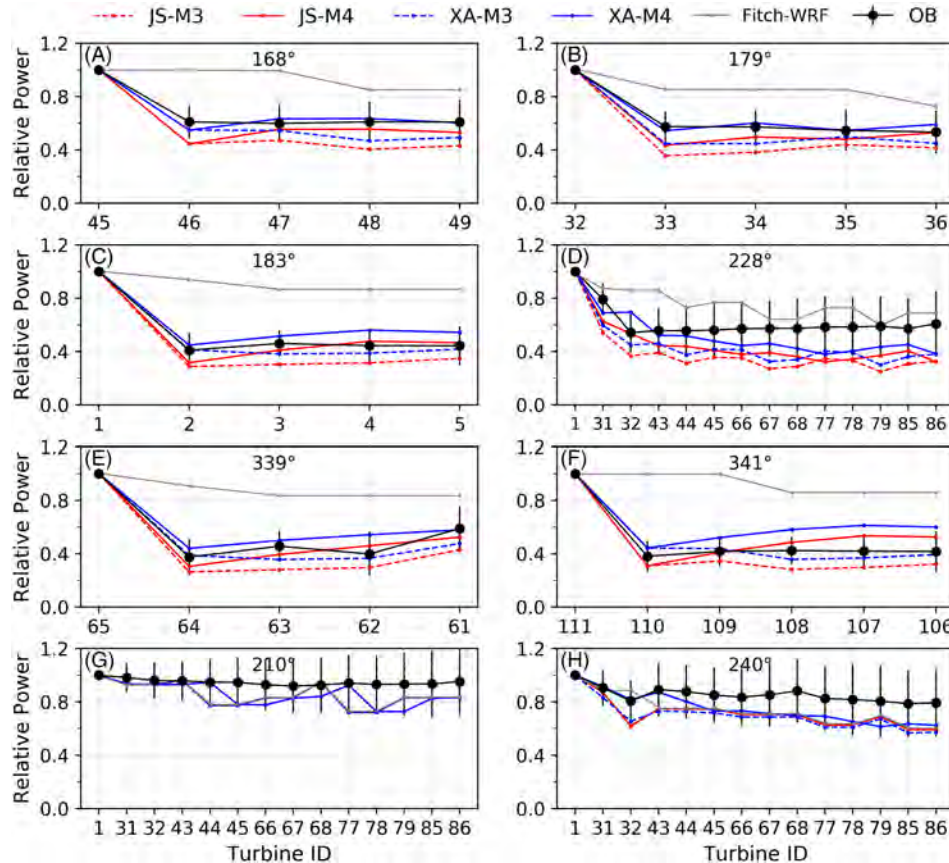


**FIGURE 7** Same as Figure 6 but at Anholt (multi-cell cases at 2-km resolution). The directions of non-alignment are 210° (G) and 240° (H)

Figures 6 and 7 show the relative power predicted by Jensen (hereafter referred to as JS) and XA for the multi-cell cases at Lillgrund and Anholt, respectively. Results obtained with the Fitch WFP are also included for comparison. Comparing relative power predicted by the two superposition methods with the same wake loss model, significant differences are observed with both models, indicating a great impact of the wake superposition method, in line with Ma and Archer<sup>16</sup> This impact seems to be more pronounced for the XA model, especially at Lillgrund, where the XA model with M4 (hereafter referred to as XA-M4) predicts not only a much higher relative power than XA-M3, but also higher than all the other combinations and higher than the observations. For the other three combinations (i.e., JS-M3, JS-M4, and XA-M3), their predictions are fairly close to one another at the two wind farms. A general trend is for method M4 to predict higher relative power than method M3 for both the Jensen and the XA wake models (as the solid lines are always above the dashed lines for each color in Figures 6 and 7). A second general trend is for wake model XA to predict higher relative power than Jensen for any given wake overlapping method (as the blue lines are always above the red lines for each line type in Figures 6 and 7). The same general trends are found in the single-cell results in Figures 8 and 9.

A statistical performance analysis based on bias and RMSE (Tables 1 to 4) indicates that the bias is generally negative for multi-cell cases and (slightly) positive for single-cell cases. The Fitch WFP is the exception, as it always exhibits a strong positive bias in all cases, but especially for single-cell cases, for which it predicts no wake losses at all. For example, all combinations at Anholt exhibit an average bias that is between -12.8% and -0.7% for multi-cell cases (column "All"), whereas for single-cell cases most combinations exhibit a positive bias (between +1.2% and +7.1%) and only JS-M3 has a slightly negative bias of -3.4%. We note that the results in column "All" are just the simple average of the results obtained for the wind directions considered here, without including information on the wind rose. The generally (slightly) positive bias of these three wake loss models was also reported by Archer et al,<sup>24</sup> which confirms that the WFPs were properly inserted in the WRF model and behave consistently with their original formulations. Positive biases are a concern because they lead (and have led in the past) to over-estimates of the wind farm power. The fact that the bias reverses sign just by redistributing the wind turbines over multiple cells is the consequence of the resolved wake, which, as discussed earlier, decreases the grid cell average wind speed incrementally at downwind grid cells with turbines. The

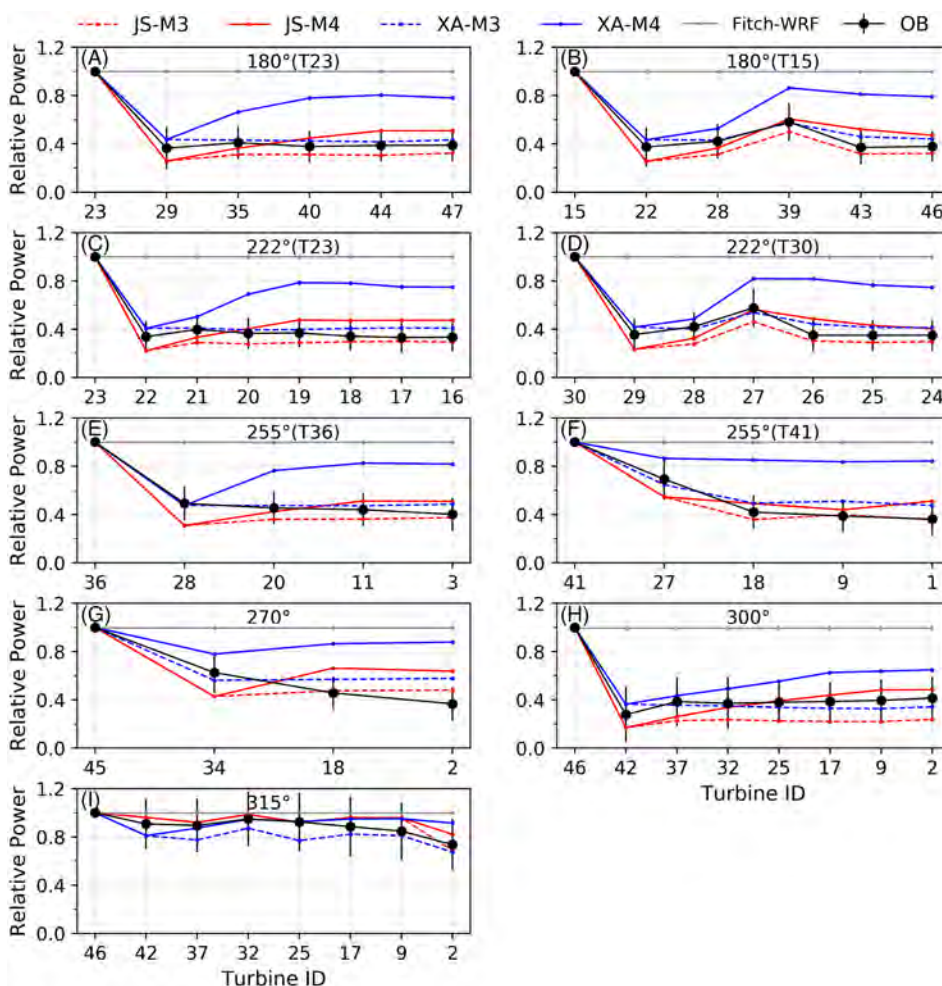
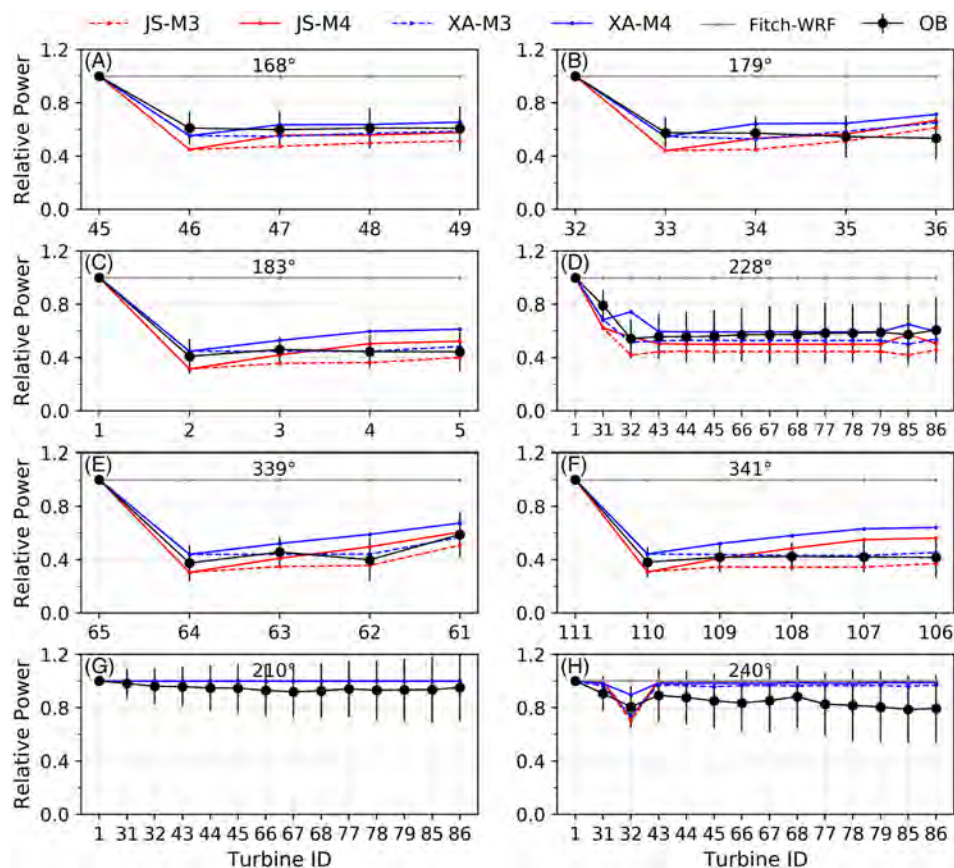


FIGURE 8 Same as Figure 6 at Lillgrund but for the single-cell cases at 4-km resolution



**FIGURE 9** Same as Figure 6 but at Anholt (single-cell cases at 24-km resolution). The directions of non-alignment are 210° (G) and 240° (H)

sub-grid wake model already takes into account the advection, diffusion, and expansion of the individual wakes. Thus the effect of the resolved wake is in addition to that of the wake loss model and may cause an excessive decrease of the total power output (thus a negative bias).

The single-cell results are generally more accurate, with a smaller RMSE than their multi-cell counterpart, except for the Fitch WFP. For example, all combinations at Anholt exhibit an average RMSE that is between 9.1% and 14.4% for multi-cell cases (column “All”), whereas for single-cell cases all combinations exhibit a lower RMSE (between 5.3% and 9.4%) and only XA-M4 is worse in the single-cell case. At Lillgrund, the RMSE is comparable in both cases. This worsening of the accuracy from single- to multi-cell cases is another consequence of the resolved wake.

At Lillgrund, the best two combinations are consistently JS-M4 and XA-M3 for both single- and multi-cell cases, while the combination XA-M4 predicts unrealistically high power (Tables 1 and 3). At Anholt, the performance of the various combinations is not as consistent between single- and multi-cell cases as it was at Lillgrund. For example, for multi-cell cases XA-M4 performs the best, with much smaller bias and RMSE than the others, while JS-M4 and XA-M3 exhibit close errors (Table 2); however, XA-M4 performs poorly for single-cell simulations (largest positive bias and RMSE in Table 4). This inconsistency at Anholt can be explained by two compensating errors. The first is the negative bias associated with the partitioning of the turbines over multiple cells discussed above; the second is the tendency of XA-M4 to over-estimate the power (based on the single-cell cases). These two effects happen to balance each other out to give the most realistic prediction with XA-M4 at Anholt for multi-cell cases.

By contrast, among the other three combinations at both farms, JS-M3 tends to greatly under-predict the power at both farms for single- and multi-cell cases.

For directions of non-alignment (i.e., 315° at Lillgrund and 240° and 210° at Anholt), at both wind farms most combinations under-predict relative power (i.e., negative biases) and exhibit relatively large RMSE in the multi-cell cases (Tables 1 and 2). In addition, the relative power continuously decreases along the column (Figures 6I and 7G,H). However, for the single-cell simulations at Anholt (Figure 9G,H and Table 4), a consistent over-prediction of relative power was found for directions of non-alignment, as all combinations predicted no wake effects at any turbine (for 210°) or after the third turbine (for 240°). This is because there is no resolved wake affecting any turbines for directions of non-alignment and therefore neither the decrease in power along the column nor the general underestimation are present in single-cell results.

A similar (unrealistic) decrease in relative power along a column can happen in multi-cell cases for directions of alignment at long columns of turbines, such as 228° at Anholt (Figure 7D). Once again, it is due to the resolved wake, which in this case artificially interferes with the effects of

**TABLE 1** Bias and root-mean-square error (RMSE) in power prediction (in percent) at Lillgrund (multi-cell case at 2-km resolution) by the Fitch parameterization, the Jensen (JS) and XA models with the wake overlap methods M3 and M4, the GM, and the ensemble of the three selected parameterizations (EWFP), each of which is marked with an asterisk (\*)

Model	180°(T23)		180°(T15)		222°(T23)		222°(T30)		255°(T36)	
	Bias	RMSE	Bias	RMSE	Bias	RMSE	Bias	RMSE	Bias	RMSE
Fitch	42.2	47.9	35.4	41.1	43.0	48.3	34.8	39.9	26.9	32.9
JS-M3	-9.7	11.3	-11.1	12.4	-10.2	11.2	-12.6	13.7	-13.8	15.9
JS-M4*	2.3	8.3	0.8	8.3	3.7	8.9	-1.4	7.7	<b>-1.8</b>	8.8
XA-M3*	<b>-0.1</b>	6.0	-2.2	5.7	<b>-0.9</b>	5.5	-3.7	6.6	-5.8	8.8
XA-M4	24.9	29.5	20.4	25.6	26.3	30.6	21.2	26.5	18.9	24.8
GM*	3.4	6.7	<b>-0.4</b>	5.8	3.3	6.6	<b>-1.3</b>	6.5	-4.0	6.9
EWFP	1.8	<b>3.8</b>	-0.6	<b>1.7</b>	2.0	<b>3.3</b>	-2.2	<b>3.8</b>	-3.9	<b>5.0</b>
Model	255°(T4)		270°		300°		315° (Non-Al.)		All°	
	Bias	RMSE	Bias	RMSE	Bias	RMSE	Bias	RMSE	Bias	RMSE
Fitch	16.4	18.6	19.7	24.0	40.1	43.9	4.4	8.1	29.2	33.9
JS-M3	-13.8	16.0	-10.9	13.8	-16.4	17.9	-2.1	5.7	-11.2	13.1
JS-M4*	<b>-2.9</b>	<b>7.3</b>	<b>1.8</b>	13.6	-3.0	6.6	-1.1	4.9	<b>-0.2</b>	8.3
XA-M3*	-8.0	9.5	-4.8	7.1	-7.3	9.8	-12.5	14.0	-5.0	8.1
XA-M4	19.6	23.4	21.4	26.1	11.0	13.0	<b>-0.1</b>	<b>4.9</b>	18.2	22.7
GM*	-8.5	10.8	-5.7	7.1	<b>-1.5</b>	5.6	-9.0	10.4	-2.6	7.4
EWFP	-6.5	8.5	-2.9	<b>6.3</b>	-4.0	<b>5.1</b>	-7.5	9.1	-2.6	<b>5.2</b>

Note: The columns in the table correspond to the wind directions in Figure 1A; the front turbine is listed in parenthesis for wind directions with multiple turbine columns. The direction 315° is a direction of non-alignment. The averages of all directions are shown in column "All." The values associated with the best performing parameterization for each direction and for each parameter are in bold.

**TABLE 2** Same as Table 1 but for Anholt (multi-cell case at 2-km resolution)

Model	168°		179°		183°		228°		339°	
	Bias	RMSE	Bias	RMSE	Bias	RMSE	Bias	RMSE	Bias	RMSE
Fitch	25.1	28.9	19.9	22.6	35.0	39.4	13.5	16.5	31.1	36.0
JS-M3	-13.5	15.3	-12.7	14.8	-10.1	11.4	-23.0	24.3	-11.0	12.6
JS-M4*	-6.8	8.7	-5.7	7.7	-1.8	5.1	-16.6	18.4	-2.7	5.8
XA-M3*	-7.4	9.0	-7.7	9.1	-3.2	4.5	-17.5	18.9	-4.6	6.9
XA-M4	<b>-0.2</b>	<b>3.4</b>	<b>1.1</b>	<b>3.2</b>	6.2	7.5	<b>-9.8</b>	<b>13.6</b>	4.9	7.3
GM*	-8.5	10.1	-6.8	8.3	<b>-0.2</b>	2.8	-18.5	20.0	<b>-2.5</b>	6.8
EWFP	-7.6	8.7	-6.8	8.2	-1.7	<b>2.7</b>	-17.5	18.9	-3.3	<b>5.7</b>
Model	341°		210° (Non-Al.)		240° (Non-Al.)		All°			
	Bias	RMSE	Bias	RMSE	Bias	RMSE	Bias	RMSE		
Fitch	41.7	46.3	-9.6	-12.2	-12.2	14.7	18.1	27.1		
JS-M3	-8.4	9.5	-9.6	12.2	-14.0	15.3	-12.8	14.4		
JS-M4*	3.4	7.5	-9.6	12.3	-14.0	15.2	-6.7	10.1		
XA-M3*	<b>-1.0</b>	4.4	-9.6	12.2	-15.6	16.6	-8.3	10.2		
XA-M4	11.7	13.6	<b>-9.0</b>	<b>11.4</b>	<b>-10.2</b>	<b>12.5</b>	<b>-0.7</b>	<b>9.1</b>		
GM*	2.8	5.2	-9.5	12.2	-14.4	15.8	-7.2	10.2		
EWFP	1.7	<b>2.3</b>	-9.6	12.2	-14.7	15.8	-7.4	9.3		

Note: The directions 210° and 240° are directions of non-alignment.

**TABLE 3** Same as Table 1 for Lillgrund, but for the single-cell case at 4-km resolution

Model	180° (T23)		180° (T15)		222° (T23)		222° (T30)		255° (T36)	
	Bias	RMSE	Bias	RMSE	Bias	RMSE	Bias	RMSE	Bias	RMSE
Fitch	51.2	56.1	47.9	53.0	56.5	60.5	51.4	56.0	44.2	49.5
JS-M3	-7.0	7.8	-7.0	8.0	-6.4	7.4	-7.7	9.1	-7.7	9.9
JS-M4*	2.6	8.9	1.5	9.1	4.7	10.5	0.6	8.7	-0.7	10.1
XA-M3*	3.5	4.2	3.5	5.1	4.5	5.3	3.2	5.7	2.4	4.1
XA-M4	25.6	30.5	21.7	27.7	27.4	32.3	23.5	29.6	21.9	28.9
GM*	6.7	7.4	4.8	6.8	8.7	9.5	5.6	8.0	3.4	4.8
EWFP	4.3	5.4	3.3	5.6	6.0	7.5	3.1	6.2	1.7	5.6
Model	255° (T4)		270°		300°		315° (Non-Al.)		All°	
	Bias	RMSE	Bias	RMSE	Bias	RMSE	Bias	RMSE	Bias	RMSE
Fitch	42.8	49.3	38.7	45.7	54.9	58.8	10.7	12.9	44.3	49.1
JS-M3	-4.0	7.1	-1.6	11.4	-13.4	14.5	3.2	5.6	-5.7	9.0
JS-M4*	2.5	10.2	7.0	19.7	-0.6	7.4	4.8	6.1	2.5	10.1
XA-M3*	5.3	8.4	6.5	12.3	-2.6	5.4	-7.6	8.9	2.1	6.6
XA-M4	30.7	36.1	26.8	33.6	14.3	16.8	2.8	8.4	21.6	27.1
GM*	4.1	10.2	4.1	10.5	3.7	5.5	-3.8	5.4	4.1	7.6
EWFP	4.0	9.3	5.9	14.1	0.2	2.0	-2.3	4.1	2.9	6.6

**TABLE 4** Same as Table 1, but for Anholt (single-cell case at 24-km resolution)

Model	168°		179°		183°		228°		339°	
	Bias	RMSE	Bias	RMSE	Bias	RMSE	Bias	RMSE	Bias	RMSE
Fitch	31.5	35.2	35.3	39.7	44.9	50.2	38.2	40.0	43.7	49.4
JS-M3	-9.9	11.3	-4.2	9.0	-6.5	7.6	-12.4	13.0	-6.0	7.1
JS-M4*	-5.7	7.9	-0.4	8.7	0.1	6.4	-6.4	7.9	-0.0	5.8
XA-M3*	-3.4	4.0	1.7	6.0	1.3	2.5	-4.8	5.4	1.4	3.7
XA-M4	1.0	3.9	6.4	9.8	8.5	10.7	2.4	6.7	8.1	10.2
GM*	-4.8	5.6	2.2	7.3	4.4	5.3	-6.8	8.0	3.4	6.3
EWFP	-4.6	5.6	1.1	7.0	1.9	3.4	-6.0	7.0	1.6	3.8
Model	341°		210° (Non-Al.)		240° (Non-Al.)		All°			
	Bias	RMSE	Bias	RMSE	Bias	RMSE	Bias	RMSE		
Fitch	49.1	53.8	5.3	5.7	14.8	15.8	32.9	36.2		
JS-M3	-5.8	6.4	5.3	5.7	12.5	15.1	-3.4	9.4		
JS-M4*	4.2	8.9	5.3	5.7	12.8	15.0	1.2	8.3		
XA-M3*	2.3	3.1	5.2	5.6	9.9	11.9	1.7	5.3		
XA-M4	12.6	15.0	5.2	5.6	12.7	13.7	7.1	9.4		
GM*	6.0	6.9	5.3	5.7	12.2	15.5	2.7	7.6		
EWFP	4.2	5.1	5.2	5.7	11.6	14.1	1.9	6.5		

Note: The directions 210° and 240° are directions of non-alignment.

the sub-grid wakes, already accounted for by the WFP. When the turbines are aligned behind each other, the WFP correctly accounts for the sub-grid wakes; the additional reduction in wind speed caused by the resolved wake in multi-cell cases is small but it grows for each additional grid cell with turbines, ultimately causing an excessive and noticeable power reduction. This is the only fundamental issue of using the approach proposed here. This effect is significant for long columns of wind turbines, regardless of the wind direction (i.e., aligned or non-aligned).

### 5.3 | Individual models versus ensemble

The simulation results in Figures 6–9 suggest that the combination JS-M3 should be excluded from the ensemble mean, because it always under-predicts the relative power. The combination XA-M4 should also be considered with caution, because it significantly over-predicts the power at tightly-spaced wind farms. Thus, we will select JS-M4 and XA-M3 for the further ensemble average, as well as the GM.

The next step is to develop an effective strategy for the ensemble averaging. A natural choice for the ensemble average is to assign weights to the individual model results. The weight should be based on the performance of the model: large weight for the better performing model and small weight for the worse performing model. However, since the performance of the models are not consistent at different wind farms and along different columns, here we assume that the weights are equal for all the ensemble members (i.e., equal to 1/3). Alternative strategies to select the ensemble weights, such as weighing by directional sector or by wind regime, may be tested in the future. The ensemble averaging is applied at each time step in the WRF model, thus the calculated velocity tendencies and turbine-induced TKE are all generated by the ensemble averaging.

The relative power from the EWFP and from the three individual WFPs are shown in Figures 10 and A.1–A.3 in the Appendix. Comparing the three individual WFP results, again none of them is clearly much better than the others. For example, JS-M4 always under-predicts the power at the second turbine and tends to over-predict the power at the last few turbines. XA-M3 tends to under-predict the power at the last few turbines. The performance of the GM model is the most consistent, with the predicted power varying around the observations, always within the error bar.

The ensemble parameterization always gives a value between the maximum and minimum of three individual WFPs for all the turbines, as expected. In comparison to the observations, the EWFP often seems to better match the observed relative power at most turbines. However, for certain columns, it predicts slightly worse results than the best performing individual wake loss model. Examples are direction 315° at Lillgrund (Figure 10I and Table 1) and 341° at Anholt (Figure A.3F and Table 4). Recall that the reason we propose the ensemble approach is that there is not a single combination that always performs better than the others in all situations (i.e., different wind farms and different wind directions). The

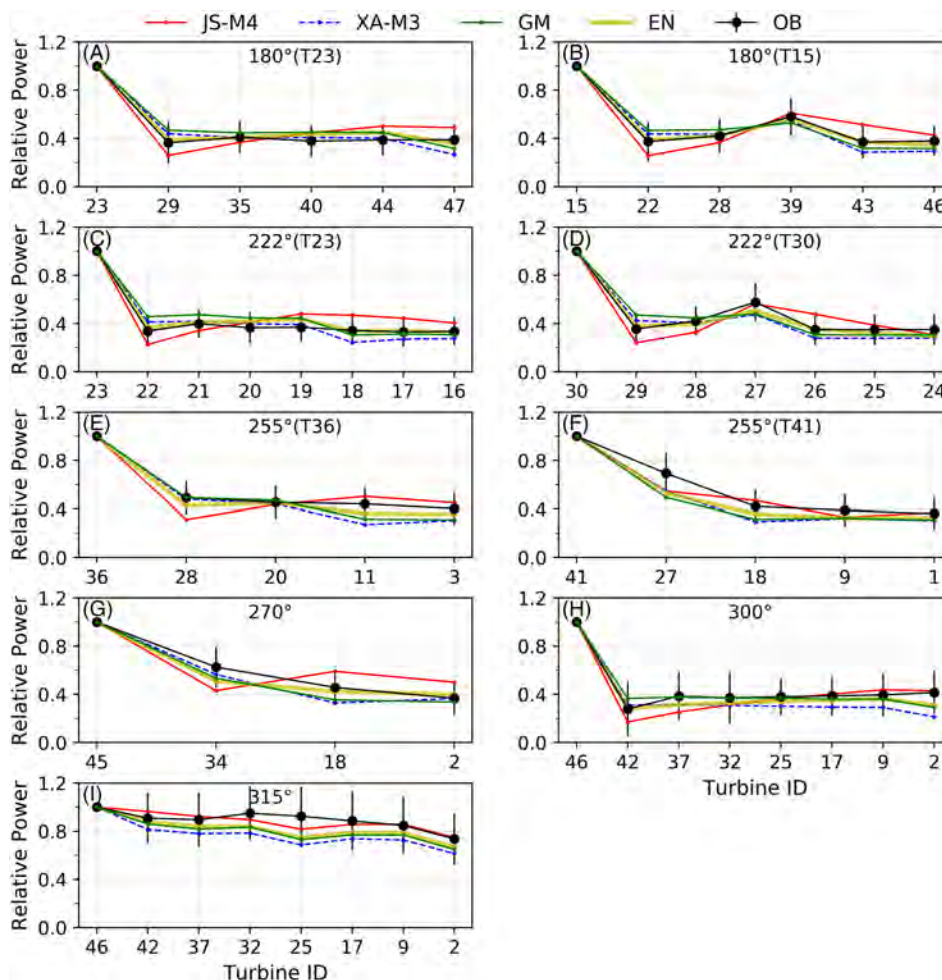


**FIGURE 10** Same as Figure 6 at Lillgrund (multi-cell cases at 2-km resolution), but for Jensen with M4, XA with M3, GM, and the ensemble of all three (EWFP)

sacrifice of obtaining a worse ensemble prediction for a few rare cases is worthwhile, since the ensemble in general provides more reliable results than any individual wake loss model.

With the ensemble averaging, the three wake loss models are run simultaneously. Compared to the simulations with one wake loss model in the wind farm parameterization scheme, this ensemble procedure inevitably increases the computational time. To examine this additional cost, we reran the 168° case (2-km resolution) at Anholt with EWFP and XA-M3. The average time required for a time step with the EWFP is about 0.232 s and that with XA-M3 is about 0.226 s, thus a modest increase of about 2.7%.

Lastly, the results of single-cell cases are, in general, more accurate than those of multi-cell cases, even for the EWFP. Comparing Tables 1 and 3 for Lillgrund and Tables 2 and 4 for Anholt, bias and RMSE are lower with single-cell results in general (e.g., XA-M3 exhibits a lower RMSE with single-cell than multi-cell simulations for eight out of nine columns at Lillgrund and for seven out of eight at Anholt), and in particular for directions of non-alignment (e.g., all combinations perform better for 210° and 240° at Anholt in single- than in multi-cell simulations) and for long columns (e.g., 228° at Anholt). This, again, can be explained by the resolved wake. The implication is that finer resolution, which requires that the wind farm be partitioned across multiple grid cells (i.e., multi-cell simulations), does not guarantee more accurate results with the WFPs proposed here. By contrast, the Fitch parameterization performs incrementally better as the resolution becomes finer,<sup>16</sup> simply because the resolved wake is resolved better. For example, the average RMSE of the Fitch WFP drops from 49.1% to 33.9% at Lillgrund (Table 1 vs. Table 3) and from 36.2% to 27.1% at Anholt (Table 2 vs. Table 4) when the resolution is increased from single-cell to multi-cell simulations.

## 6 | CONCLUSIONS AND RECOMMENDATIONS

We propose a set of new WFPs that account for sub-grid wakes from wind turbines within the same grid cell via a combination of a wake model—Jensen, GM, or XA—and a wake superposition method—M3 or M4. We also propose an ensemble approach, in which several WFPs are run simultaneously and their combined effect is then fed back to the resolved processes of the model. We use observed data from two operational wind farms, Lillgrund and Anholt, to evaluate the performance of the various WFPs that are created by combining different wake models and wake overlapping methods. We also assess the effects of increasing the grid resolution by simulating both single-cell cases, in which the wind farm is entirely contained in a computational grid cell, and multi-cell cases, in which the wind farm is partitioned across multiple grid cells of 2 km by 2 km.

We find that all the proposed WFPs perform well (overall bias between -11.0% and 21.6% and overall RMSE between 5.3% and 27.1%) and that no individual WFP, not even the ensemble WFP, outperforms all others for all wind directions, farms, and resolutions. As such, we are not able to make universal recommendations on which WFP to use for which case. However, we report three general trends that may be useful to other researchers in selecting the right combinations of a wake model and a wake superposition method in the WFP for future applications:

- (1) For a given wake model, wake superposition method M4 predicts higher relative power than method M3;
- (2) For a given wake superposition method, the XA wake model predicts higher relative power than the Jensen model;
- (3) For any given WFP, the partitioning of the wind farm over multiple grid cells generally causes a reduction in the power prediction (and often a switch in the sign of the bias from positive with single-cell cases to negative for multi-cells cases), due to the resolved wake. The resolved wake causes an unrealistic incremental wind speed reduction with each downstream grid cell with turbines due to the combination of advection and additional momentum extraction by the turbines, which is not observed in real wind farms (where the wind speed deficit is observed to stabilize after the first few rows of turbines). It is a numerical effect caused by the fact that, in the absence of a sub-grid wake model, the entire downstream grid cell, as opposed to only the portion that is affected by upstream wakes, experiences a reduced wind speed.

These three findings indicate that certain combinations may be less likely to be satisfactory. For example, XA+M4 is more likely to introduce a positive bias, while JS+M3 a negative bias. This is not to say that these two combinations should not be used at all, but rather that they need to be carefully considered depending on the circumstances. For example, at Anholt in the multi-cell cases, XA+M4 was often the best performing combination because the partitioning of the wind farm, which causes an under-prediction of power, was compensated for by the over-prediction of power by XA+M4.

In terms of the EWFP, it generally performs well, with overall bias between -3.3% and 7.1% and RMSE between 5.2% and 9.3%. Our findings suggest that the EWFP performs better at tightly packed wind farms, like Lillgrund, than at widely spaced and efficient wind farms, like Anholt. Because we had observational data at our disposal, we were able to select a subset of WFPs for the ensemble that were already performing well on their own, based on bias and RMSE. This is the strategy that we recommend if observations are available. If one specific WFP outperforms the others in all or most cases, then we do not recommend the use of the EWFP approach because the added computational cost, although generally small, may not be worth it. For example, for the single-cell cases at Anholt, it appears that XA+M3 is a better choice than the EWFP. If observations are not available—for example, for future wind farms—then we recommend that the EWFP include the three WFPs that we used here, namely XA with M3, Jensen with M4, and the GM, because they perform well in general and because they offer a good mix of over- and under-prediction tendencies that are beneficial to the ensemble.

We conclude that the use of a wake model and a wake superposition model in a WFP for the WRF model is potentially advantageous because it generates accurate wind power predictions, especially with the ensemble approach. We note that, however, in the multi-cell cases, the effects of the sub-grid wakes from the WFP are added on to the resolved wake effects in a manner that is not entirely correct (there is no such double-counting issue in the single-case cases). This issue needs to be investigated further. A possible solution would be to suppress the resolved-scale advection and diffusion processes entirely at the grid cells where the wind turbines are located, preferably within the WFP. Alternatively, choosing a resolution fine enough to allow for only one turbine per grid cell and using the Fitch parameterization would avoid the double-counting issue because only the resolved wake effects would be accounted for and not the sub-grid wake effects.

Another potential issue is the treatment of the added TKE by the wakes. The proposed WFPs only deal with the wind speed deficit, while the added TKE is treated exactly like in the Fitch parameterization, that is, via an additional term in the TKE equation that is proportional to the difference between the thrust and power coefficients of the wind turbine. We plan to use the method proposed by Volker et al<sup>40</sup> to treat the added TKE with these new WFPs in the future.

## ACKNOWLEDGEMENTS

This research was funded by the U.S. Bureau of Ocean Energy Management (BOEM), project no. 0040420490. The simulations were conducted on the Caviness high-performance computer cluster of the University of Delaware.

## DATA AVAILABILITY STATEMENT

All codes developed as part of this paper will be made available to interested parties upon request. The authors intend to make the codes also available through the official WRF repository.

## ORCID

Cristina L. Archer  <https://orcid.org/0000-0002-7837-7575>

## REFERENCES

- Lee J, Zhao F. GWEC – Global Wind Report 2021, Brussels, Belgium, Global Wind Energy Council; 2021. <https://gwec.net/global-wind-report-2021/>
- Wind Energy Landscapes. Horse Hollow – Details. <https://www.maclester.edu/windenergy/casestudies/horsehollow/HHdetails.html>, Accessed: 2021-08-08; 2008.
- Khan MA, Javed A, Shakir S, Syed AH. Optimization of a wind farm by coupled actuator disk and mesoscale models to mitigate neighboring wind farm wake interference from repowering perspective. *Appl Energy*. 2021;298:117229.
- Skamarock WC, Klemp JB, Dudhia J, Gill DO, Barker D, Duda MG, yu Huang X, Wang W, Powers JG. A description of the advanced research WRF version 3, Boulder, Colorado, USA, University Corporation for Atmospheric Research; 2008.
- Fitch AC, Olson JB, Lundquist JK, Dudhia J, Gupta AK, Michalakes J, Barstad I. Local and mesoscale impacts of wind farms as parameterized in a mesoscale NWP model. *Monthly Weather Rev*. 2012;140(9):3017-3038.
- Pryor SC, Shepherd TJ, Barthelmie RJ, Hahmann AN, Volker P. Wind farm wakes simulated using WRF. *J Phys: Confer Ser*. 2019;1256:12025.
- Prosper MA, Otero-Casal C, Fernandez FC, Miguez-Macho G. Wind power forecasting for a real onshore wind farm on complex terrain using WRF high resolution simulations. *Renew Energy*. 2019;135:674-686.
- Siedersleben SK, Platis A, Lundquist JK, et al. Turbulent kinetic energy over large offshore wind farms observed and simulated by the mesoscale model WRF (3.8.1). *Geosci Model Develop*. 2020;13(1):249-268.
- Boezio GC, Ortelli S. Use of the WRF-DA 3D-var data assimilation system to obtain wind speed estimates in regular grids from measurements at wind farms in uruguay. *Data*. 2019;4(4):142.
- Duarte Jacondino W, Nascimento ALDS, Calvetti L, Fisch G, Augustus Assis Beneti C, da Paz SR. Hourly day-ahead wind power forecasting at two wind farms in northeast brazil using WRF model. *Energy*. 2021;230:120841.
- Pan Y, Archer CL. A hybrid wind-farm parametrization for mesoscale and climate models. *Bound-Layer Meteorol*. 2018;168(3):469-495.
- Wang C, Jin S. Error features and their possible causes in simulated low-level winds by WRF at a wind farm. *Wind Energy*. 2014;17(9):1315-1325.
- Archer CL, Wu S, Ma Y, Jiménez P. Two corrections for the treatment of turbulent kinetic energy in the WRF model. *Monthly Weather Rev*. 2020;148(12):4823-4835.
- Fitch AC. Notes on using the mesoscale wind farm parameterization of fitch et al. (2012) in WRF. *Wind Energy*. 2016;19(9):1757-1758.
- Jiménez PA, Dudhia J, González-Rouco JF, Navarro J, Montávez JP, García-Bustamante E. A revised scheme for the WRF surface layer formulation. *Monthly Weather Rev*. 2012;140(3):898-918.
- Ma Y, Archer CL. A Jensen-based wind farm parameterization for the WRF and MPAS models. In: American Meteorological Society (AMS) 101st Annual Meeting, Vol. Joint 4.ii.2; 2021; Online. <https://ams.confex.com/ams/101ANNUAL/meetingapp.cgi/Paper/379813>
- Adams AS, Keith DW. Wind energy and climate: Modeling the atmospheric impacts of wind energy turbines. In: American Geophysical Union (AGU) Fall Meeting, Vol. B44B-08; 2007; San Francisco, California, USA.
- Adams AS, Keith DW. Are global wind power resource estimates overstated? *Environ Res Lett*. 2013;8(1):15021.
- Volker PJH, Badger J, Hahmann AN, Ott S. The explicit wake parametrisation v1.0: A wind farm parametrisation in the mesoscale model WRF. *Geosci Model Develop*. 2015;8(11):3715-3731.
- Shepherd TJ, Barthelmie RJ, Pryor SC. Sensitivity of wind turbine array downstream effects to the parameterization used in WRF. *J Appl Meteorol Climatol*. 2020;59(3):333-361.
- Mayol ML, Saulo AC, Otero AD. Farm to farm wake interaction in WRF: impact on power production. *J Phys: Confer Ser*. 2021;1934(1):12017.

22. Santoni C, Garcia-Cartagena EJ, Ciri U, Iungo GV, Leonardi S. Coupling of mesoscale weather research and forecasting model to a high fidelity large eddy simulation. *J Phys: Confer Ser.* 2018;1037(6):62010.
23. Elshafei B, Pena A, Xu D, Ren J, Badger J, Pimenta FM, Giddings D, Mao X. A hybrid solution for offshore wind resource assessment from limited onshore measurements. *Appl Energy.* 2021;298:117245.
24. Archer CL, Vassel-Be-Hagh A, Yan C, Wu S, Pan Y, Brodie JF, Maguire AE. Review and evaluation of wake loss models for wind energy applications. *Appl Energy.* 2018;226:1187-1207.
25. Ghaisas NS, Archer CL. Geometry-based models for studying the effects of wind farm layout. *J Atmos Ocean Technol.* 2016;33(3):481-501.
26. Katic I, Højstrup J, Jensen NO. A simple model for cluster efficiency. In: European Wind Energy Association Conference and Exhibition; 1986: 407-410.
27. Xie S, Archer C. Self-similarity and turbulence characteristics of wind turbine wakes via large-eddy simulation. *Wind Energy.* 2015;18(10):1815-1838.
28. Lissaman PBS. Energy effectiveness of arbitrary arrays of wind turbines. *J Energy.* 1979;3(6):323-328.
29. Voutsinas S, Rados K, Zervos A. On the analysis of wake effects in wind parks. *Wind Eng.* 1990;14(4):204-219.
30. Lanzilao L, Meyers J. A new wake-merging method for wind-farm power prediction in the presence of heterogeneous background velocity fields. *Wind Energy.* 2022;25(2):237-259.
31. Choukulkar A, Pichugina Y, Clack CTM, Calhoun R, Banta R, Brewer A, Hardesty M. A new formulation for rotor equivalent wind speed for wind resource assessment and wind power forecasting. *Wind Energy.* 2016;19(8):1439-1452.
32. St. Pé A, Sperling M, Brodie JF, Delgado R. Classifying rotor-layer wind to reduce offshore available power uncertainty. *Wind Energy.* 2018;21(7): 461-473.
33. DiDonato AR, Jarnagin MP. Integration of the general bivariate Gaussian distribution over an offset circle. *Math Comp.* 1961;15:375-382.
34. Porté-Agel F, Bastankhah M, Shamsoddin S. Wind-turbine and wind-farm flows: a review. *Bound-Layer Meteorol.* 2020;174(1):1-59.
35. Nakanishi M, Niino H. Development of an improved turbulence closure model for the atmospheric boundary layer. *J Meteorol Soc Japan.* 2009;87(5): 895-912.
36. Jiménez PA, Navarro J, Palomares AM, Dudhia J. Mesoscale modeling of offshore wind turbine wakes at the wind farm resolving scale: a composite-based analysis with the Weather Research and Forecasting model over Horns Rev. *Wind Energy.* 2015;18:559-566.
37. Eriksson O, Lindvall J, Breton S-P, Ivanell S. Wake downstream of the Lillgrund wind farm - A comparison between LES using the actuator disc method and a wind farm parametrization in WRF. *J Phys.* 2015;625(1):12-28.
38. Dahlberg J-AA. Assessment of the Lillgrund windfarm. 6\_1 LG Pilot Report, Stockholm, Sweden, Vattenfall; 2009. Available at <https://www.osti.gov/etdeweb/servlets/purl/979747>
39. Barthelmie RJ, Pryor SC, Frandsen ST, et al. Quantifying the impact of wind turbine wakes on power output at offshore wind farms. *J Atmos Ocean Technol.* 2010;27(8):1302-1317.
40. Volker PJH, Badger J, Hahmann AN, Ott S. The explicit wake parametrization v1.0: A wind farm parametrization in the mesoscale model WRF. *Geosci Model Dev.* 2015;8(11):3715-3731.

**How to cite this article:** Ma Y, Archer CL, Vassel-Be-Hagh A. Comparison of individual versus ensemble wind farm parameterizations inclusive of sub-grid wakes for the WRF model. *Wind Energy.* 2022;25(9):1573-1595. doi:[10.1002/we.2758](https://doi.org/10.1002/we.2758)

## APPENDIX

This appendix contains additional figures from single-cell (i.e., all the turbines are located in the same grid cell in the WRF model) and multi-cell (i.e., the turbines are distributed across multiple grid cells) cases at both Lillgrund and Anholt. The resolution for all the multi-cell cases is 2 km. Due to the size difference between the two wind farms, the horizontal grid resolution for the single-cell cases is 4 km for Lillgrund and 24 km for Anholt.

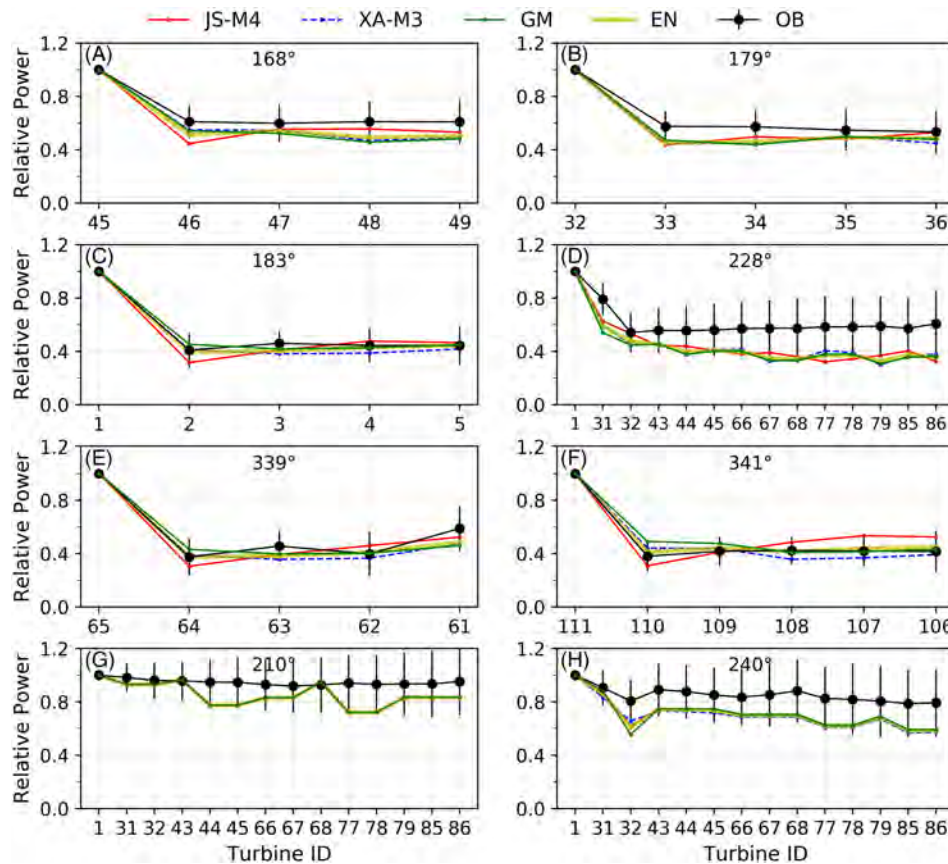


**FIGURE A.1** Relative power at Anholt (multi-cell cases at 2-km resolution) from observations and from the Jensen model with wake superposition methods M4, the XA model with M3, the GM, and the ensemble of all three (EWFP) along the directions of alignment (A–F) and the directions of non-alignment 210° and 240° (G, H). The black circles represent the mean observed relative power and the bars are one standard deviation. The simulation results and the observations are averaged over a wind direction window of  $\pm 2.5^\circ$ .

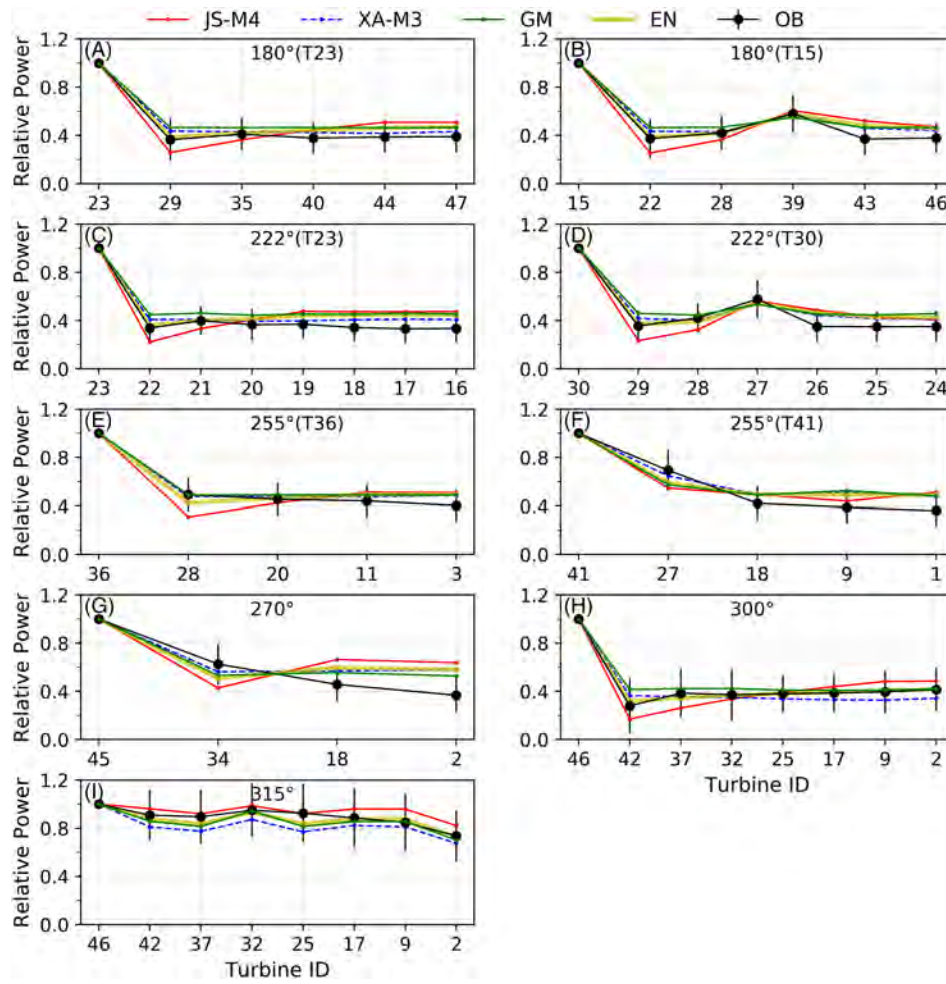


FIGURE A.2 Same as Figure A.1 but at Lillgrund for the single-cell cases at 4-km resolution. The direction of non-alignment is 315° (I)

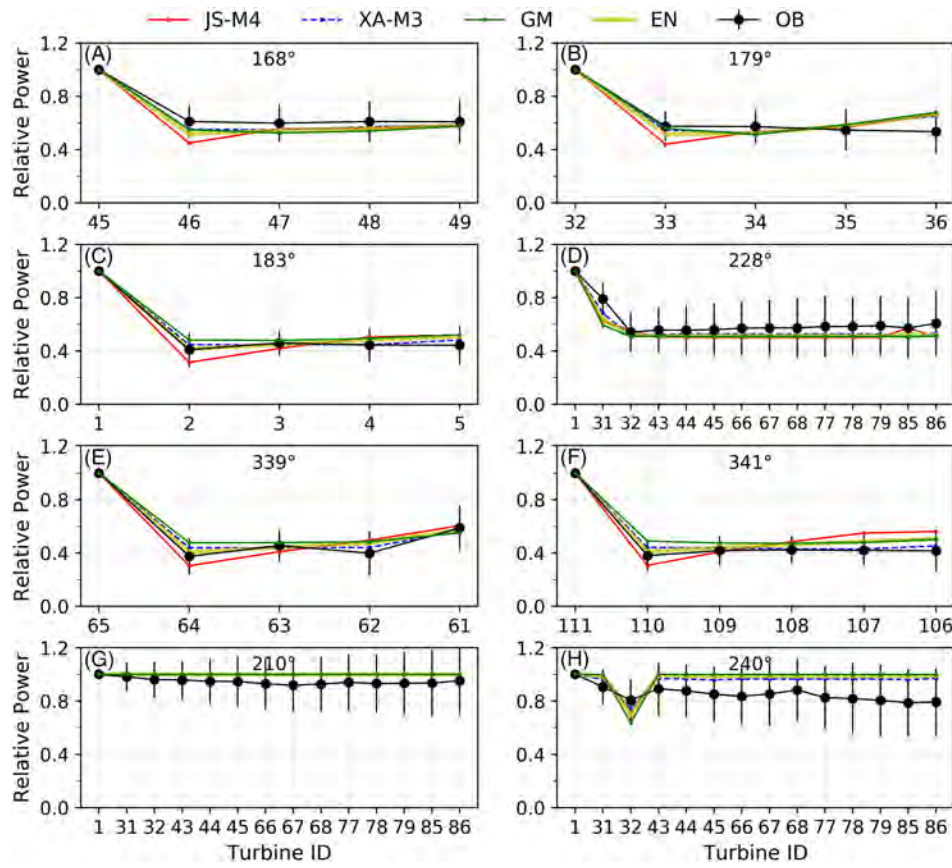


FIGURE A.3 Same as Figure A.1 at Anholt, but for the single-cell cases at 24-km resolution